DOI:
10.2967/jnumed.116.178335

Document Version
Publisher's PDF, also known as Version of record

Journal of Nuclear Medicine, published on August 17, 2017 as doi:10.2967/jnumed.116.178335

Pseudo-reference regions for glial imaging with ^{11}C-PBR28: investigation in two clinical cohorts

Daniel S. Albrecht[1,2], Marc D. Normandin[1], Sergey Shcherbinin[3], Dustin W. Wooten[2], Adam J. Schwarz[3], Nicole R Zürcher[1], Vanessa N. Barth[3], Nicolas J. Guehl[2], Oluwaseun Akeju[4], Nazem Atassi[5], Mattia Veronese[6], Federico Turkheimer[6], Jacob M. Hooker[1], Marco L. Loggia[1]

[1]A. A. Martinos Center for Biomedical Imaging, Department of Radiology, Massachusetts General Hospital, Harvard Medical School, Charlestown, MA, USA

[2]Gordon Center for Medical Imaging, NMMI, Radiology Department, Massachusetts General Hospital & Harvard Medical School,
Boston, MA, USA

[3]Eli Lilly and Company, Indianapolis, IN, USA

[4]Department of Anesthesiology, Massachusetts General Hospital, Harvard Medical School, Boston, MA, USA

[5]Neurological Clinical Research Institute, Department of Neurology, Massachusetts General Hospital, Harvard Medical School, Boston, MA, USA

[6]Department of Neuroimaging, Institute of Psychiatry, King's College London, London, United Kingdom

Corresponding author contact information:

Marco L. Loggia, PhD

A. A. Martinos Center for Biomedical Imaging

Massachusetts General Hospital

149 Thirteenth Street, Room 2301

Charlestown, MA 02129

Phone: (617) 643-7267

Fax: (617) 726-7422

Email: marco@nmr.mgh.harvard.edu

First author contact information:

Daniel S. Albrecht, PhD, Research Fellow

A. A. Martinos Center for Biomedical Imaging

Massachusetts General Hospital

149 Thirteenth Street, Room 2301

Charlestown, MA 02129

Phone: 617-643-6748

Fax: 617-726-7422

E-mail: dsalbrecht@mgh.harvard.edu

Word count: 6359

We thank the following funding sources: 1R01NS094306-01A1 (MLL), 1R01NS094306-01A1 (MLL), 1R21NS087472-01A1 (MLL), IASP Early Career Award (MLL), DoD W81XWH-14-1-0543 (MLL), Harvard Catalyst Advanced Imaging Pilot Grant (JMH), a sponsored research agreement with Eli Lilly (JMH), 5T32EB13180 (T32 supporting DSA), K23NS083715 (NA), and an Anne Young Fellowship (NA).

Running title: Pseudo-reference regions for PBR28

ABSTRACT

The translocator protein (TSPO) is a commonly used imaging target to investigate neuroinflammation. While TSPO imaging demonstrates great promise, its signal exhibits substantial interindividual variability, which needs to be accounted for to uncover group effects that are truly reflective of neuroimmune activation. Recent evidence suggests that relative metrics computed using pseudo-reference approaches can minimize within-group variability, and increase sensitivity to detect physiologically meaningful group differences. Here, we evaluated various ratio approaches for TSPO imaging and compared them with standard kinetic modeling techniques, analyzing two different disease cohorts.

Patients with chronic low back pain (cLBP) or amyotrophic lateral sclerosis (ALS) and matching healthy controls received ^{11}C-PBR28 PET scans. Occipital cortex, cerebellum and whole brain were first evaluated as candidate pseudo-reference regions by testing for the absence of group differences in Standardized Uptake Value (SUV) and distribution volume (V_T) estimated with an arterial input function (AIF). SUV from target regions (cLBP study – thalamus; ALS study – precentral gyrus) was normalized with SUV from candidate pseudo-reference regions to obtain $SUVR_{occip}$, $SUVR_{cereb}$, and $SUVR_{WB}$. The sensitivity to detect group differences in target regions was compared using various SUVR approaches, as well as distribution volume ratio (DVR) estimated with (blDVR) or without AIF (refDVR), and V_T. Additional voxelwise SUVR group analyses were performed.

We observed no significant group differences in pseudo-reference V_T or SUV, excepting whole-brain V_T, which was higher in cLBP patients than controls. Target V_T elevations in patients (p=0.028 and 0.051 in cLBP and ALS, respectively) were similarly detected by $SUVR_{occip}$ and $SUVR_{WB}$, and by refDVR and blDVR (less reliably by

$SUVR_{cereb}$). In voxelwise analyses, $SUVR_{occip}$, but not $SUVR_{cereb}$, identified regional group differences initially observed with $SUVR_{WB}$, and in additional areas suspected to be affected in the pathology examined. All ratio metrics were highly cross-correlated, but generally were not associated with V_T.

While important caveats need to be considered when using relative metrics, ratio analyses appear to be similarly sensitive to detect pathology-related group differences in ^{11}C-PBR28 signal as classic kinetic modeling techniques. Occipital cortex may be a suitable pseudo-reference region, at least for the populations evaluated, pending further validation in larger cohorts.

Keywords: Neuroinflammation, human, microglia, astrocytes, neuroimmunology.

INTRODUCTION

A growing body of work indicates that neuroinflammation, and more specifically glial activation, plays an important role in the pathophysiology of many neurological disorders, ranging from schizophrenia to chronic pain (*1*). Arguably, the most commonly evaluated targets for in vivo visualization of glial activation is TSPO (*2*). TSPO is strongly upregulated in activated microglia and reactive astrocytes during brain and spinal neuroinflammatory states (*3*), and can be imaged with PET radiotracers like ^{11}C-PBR28.

Using ^{11}C-PBR28 with classical kinetic modeling measures various groups have detected elevated PET signal in a variety of conditions with a known or suspected inflammatory component, including Alzheimer's Disease (*4,5*), human immunodeficiency virus (*6*) and epilepsy (*7*), among others. Despite these promising results, interpretation of TSPO PET signal is often complicated by substantial interindividual variability. For instance, large variability is commonly observed when ^{11}C-PBR28 binding is quantified by V_T estimation with AIF (*8*), which is considered by many to be the gold standard for

quantification of TSPO binding. Such variability, which may be associated with multiple factors not necessarily linked to neuroinflammation, including genetically-explained differences in radioligand binding affinity (*9*), variability in vascular TSPO binding (*10*), or binding to plasma protein (*11*) needs to be accounted for in order to identify group effects that are truly reflective of neuroimmune activation. However, while the effect of genotype on TSPO PET signal is well documented (*9,12,13*), the extent to which variability in vascular or plasma binding affects TSPO PET data remains to be characterized.

One way to account for such global variability is to scale ^{11}C-PBR28 uptake (either estimated using kinetic modeling or through simplified methods such as SUV) by a normalizing factor. Of course, the use of relative outcome measures precludes the absolute quantification of protein expression, which is a strength of PET imaging. However, previous work showing ratio metrics can detect group differences with similar sensitivity to traditional kinetic modeling (*4*) suggests that these approaches may be beneficial under certain circumstances. Several studies have normalized ^{11}C-PBR28 uptake with average signal of the whole brain or whole gray matter (*6,8,14-18*). While this approach may improve the detection of focal effects by robustly reducing between-subject variability, it also carries a penalty in that it reduces sensitivity to detect spatially extended effects. This becomes particularly problematic when the condition investigated is characterized by global, rather than regional, inflammation (e.g., neurological disorders demonstrating widespread neurodegeneration, exposure to lipopolysaccharide challenge, etc), and thus the reference region signal will contain signal from target regions. Therefore, the identification of a more focal reference region is desirable (*4*). Due to the lack of a true TSPO reference region devoid of specific binding (*19*), a suitable pseudo-reference region, relatively unaffected by pathology, must be identified.

In the present investigation, we evaluated analytical approaches employing different pseudo-reference regions for ^{11}C-PBR28 PET imaging, and compared them with standard kinetic modeling techniques

MATERIALS AND METHODS

Study Design

In this study, we reanalyzed two disease cohorts from previously reported datasets, cLBP (*14*) and ALS (*17*), along with corresponding healthy control subjects. We evaluated cerebellum, occipital cortex, and whole brain as putative pseudo-reference regions. The cerebellum was chosen to evaluate the generalizability to other disorders of the results by Lyoo et al. (*4*), who had shown this region to be a viable pseudo-reference for ^{11}C-PBR28 studies in Alzheimer's Disease. The occipital cortex was chosen because it is thought to be relatively spared from pathology in patients suffering from either chronic pain (*20,21*) or ALS (*22,23*). The whole brain has been used to normalize signal in the original cLBP and ALS publications, as well as in other studies (*14,15,17,18*). In order to compare the effect of the regional pseudo-reference approach to the original analyses, which used SUV normalized by whole brain ($SUVR_{WB}$), the same preprocessing and group analyses from the original studies were replicated, preserving the existing across-studies differences in design and image processing.

Detailed information about the analytical strategies employed are presented below. In brief, initial characterization of candidate pseudo-reference regions was performed by testing for the absence of group differences in V_T, estimated with AIF and traditional two-tissue compartmental modeling (2TCM), and SUV. Subsequently, the sensitivity to detect SUVR ROI group differences in "target regions" [i.e. regions showing the largest group differences in the original studies; bilateral thalamus (cLBP) and

bilateral precentral gyrus (ALS)] was compared to that using V_T. Additional SUVR group analyses were performed in a whole brain voxelwise approach. The pseudo-reference region providing the greatest sensitivity to detect group differences in the preliminary SUVR analyses (i.e., occipital cortex, see Results) was then further assessed, by computing distribution volume ratio estimated with ($blDVR_{occip}$) or without AIF ($refDVR_{occip}$).

All datasets were acquired at the Athinoula A. Martinos Center for Biomedical Imaging at Massachusetts General Hospital. All protocols were approved by the Institutional Review Board and Radioactive Drug Research Committee, and all subjects signed a written informed consent.

Subjects

Demographic information from the participants has previously been published (*14,17*). Briefly, the cLBP study consisted of 10 patients and 9 healthy controls, evaluated in a matched pairs design (with two patients matched to the same control). The ALS study consisted of 10 patients and 10 controls (8 of whom were scanned as part of the cLBP study) demographically matched but not individually paired with ALS patients (Supplemental Table 1).

Image Acquisition

Ninety-minute dynamic ^{11}C-PBR28 scans were performed with an integrated PET/MRI scanner consisting of a dedicated brain avalanche photodiode-based PET scanner in the bore of a Siemens 3T Tim Trio MRI (*24*). A multi-echo MPRAGE volume was acquired prior to tracer injection (TR/TE1/TE2/TE3/TE4 = 2530/1.64/3.5/5.36/7.22 ms, flip angle = 7°, voxel size = 1mm isotropic) for the purpose of anatomical localization,

spatial normalization of the imaging data, as well as generation of attenuation correction maps (*25*). For either cohort, mean injected dose and injected mass were not significantly different across groups (Supplemental Table 1).

Arterial Plasma and Metabolite Analysis

For the first 3 minutes post-injection, arterial blood samples were collected at 6-10s intervals, followed by additional samples at 5, 10, 20, 30, 60, and 90 minutes for plasma and metabolite analysis. Parent fraction in plasma was determined as follows. Arterial blood was centrifuged immediately following collection to separate plasma. A 600μL plasma aliquot was removed and added to 600μL acetonitrile to cause protein precipitation. After centrifugation, a 300μL aliquot of supernatant was removed and diluted into 4mL water. This sample was loaded on a HyperSep C18 solid extraction cartridge (500mg media) that had been prewashed with ethanol and equilibrated with aqueous trifluoroacetic acid (0.1%). The flow through was collected as elution volume 1 and the column was eluted in 7 additional steps (4mL eluent) at the following acetonitrile percentages: 0, 10, 20, 30, 40, 70, 100, with the balance being 0.1% trifluoroacetic acid. The unmetabolized compound (assigned by control experiments) was collected in elution volumes 5 through 8. The ratio of summed radioactivity in elution volumes 5 though 8 (parent compound) was taken relative to the total radioactivity eluted to determine the parent fraction for each time point. Five plasma outliers were excluded, as they fell outside the range of median ± 2.5*median absolute deviation (*26*). Another two subjects' data were excluded due to technical complications that prevented completion of arterial sampling.

Data Analysis

Static Image Generation. 60-90 minute SUV images were generated as described previously (*14,17*). MPRAGE-based attenuation correction was performed according to published methods (*25*). SUV maps were transformed to MNI space and smoothed with an 8mm (cLBP) or 6mm (ALS) full width at half maximum Gaussian kernel, as in the respective original analyses (*14,17*). Finally, SUV frames were normalized by average uptake in cerebellum ($SUVR_{cereb}$) and occipital cortex ($SUVR_{occip}$) for comparison against previously reported $SUVR_{WB}$.

Dynamic Image Generation. Dynamic ^{11}C-PBR28 scans were reconstructed using in-house software with the following time-frames: 8x10s; 3x20s; 2x30s; 1x60s; 1x120s; 1x180s; 8x300s; 4x600s. Frame-by-frame motion correction was performed, and data were converted to SUV by dividing by injected radioactivity/lean body mass. To characterize dynamic activity in candidate pseudo-reference regions and whole brain, SUV time activity curves were extracted from images in subject-space. Dynamic data were unavailable for one control in the ALS cohort, and this subject was excluded from all dynamic analyses.

Kinetic modeling. V_T was estimated for all target and reference regions using 2TCM with a fixed blood volume of 5% (*19*). For plasma processing, parent plasma fraction curves were fitted to a bi-exponential function. Plasma curves were fitted to a tri-exponential function, and combined with interpolated parent fractions to yield a metabolite-corrected plasma curve (see Supplemental Fig. 1 for example fits for both parent fraction and plasma input function). Arterial plasma data were unavailable for one cLBP and one ALS patient (for technical difficulties during the scan, as mentioned above); therefore, these subjects were excluded from all blood-based analyses. As the occipital cortex emerged as the preferred candidate for pseudo-reference region (see

Results), we proceeded with kinetic modeling of ratio metrics using only this brain area. Occipital DVR was estimated in two ways with in-house Matlab code, both implementing Logan graphical analysis [reference-based (*27*) and blood-based (*28*)] with t*=15 minutes. First, we used the occipital time activity curve as an input function to obtain DVR ($refDVR_{occip}$). Then, we computed AIF-derived DVR ($blDVR_{occip}$) by dividing target V_T by occipital cortex V_T. We chose Logan-based methods as primary analytical approaches for ratio metrics, as in previous ^{11}C-PBR28 studies (*29,30*), because they allow a direct comparison of V_T estimations with AIF as well as blood-free pseudo-reference tissue inputs (a secondary aim in the present study).

Statistical Analysis

In order to evaluate the viability of putative pseudo-reference candidate regions, we first sought to demonstrate that PET signal in these regions was not different across groups, which would preclude their utility as pseudo-reference regions. To this end, we compared V_T and SUV across groups for cerebellum, occipital cortex, and whole brain. For SUV analyses, we used the same nonparametric tests employed in the previous publications [Wilcoxon signed rank test for cLBP (*14*); Mann-Whitney U test for ALS (*17*)]. Subsequently, we used the same statistical tests to evaluate the ability of different ROI-based analytical approaches (SUVR, refDVR) to detect group differences in target regions. Because outlier exclusion unbalanced the relative proportion of high- and mixed-affinity binders in both cLBP and ALS groups, an unpaired one-way ANOVA with group and genotype as fixed factors, and a group*genotype interaction term was used to assess group differences in blDVR and V_T.

Group differences were interrogated with target region SUVR, and compared to differences obtained with V_T. Receiver operating characteristic (ROC) curves were then

employed to further characterize the ability of each candidate pseudo-reference region to distinguish patients from controls based on mean target region SUVR, in comparison to target V_T. Area under the ROC curve (AUROC) was used as an outcome measure (AUROC=1 represents perfectly accurate group classification, or 100% specificity and sensitivity, and AUROC=0.5 indicates discriminatory power equivalent to chance). Whole brain voxelwise SUVR analyses were also performed for comparison with the $SUVR_{WB}$ data previously reported (*14,17*). Briefly, these analyses were conducted using the randomise tool from the FSL suite, with threshold-free cluster enhancement (*31*), and a corrected threshold of $p < 0.05$. Relationships between V_T, SUV, SUVR, and DVR were assessed with Pearson's *r*. In the cLBP dataset, because 2 patients matched the same control, the SUVR ROI and voxelwise group comparisons were repeated in two separate matched-pairs analyses, using one of the two patients matched control, as described previously (*14*). Because results using both patients were similar, we present here group comparisons utilizing the "best match" (in terms of age). However, because one of these two cLBP matching patients lacked arterial plasma data, the V_T and blDVR (and, for consistency, refDVR) analyses were performed only with the patient for whom these data were available. In the unpaired group and correlation analyses, all available data were used.

RESULTS

Descriptive statistics for all outcome measures are shown in Table 1.

SUV and V_T in Candidate Pseudo-reference Regions

There were no significant group differences in SUV for any of the pseudo-reference regions (Fig. 1, left). No significant group differences in V_T were observed for

occipital and cerebellar pseudo-reference regions, for either study; however, there was a significant group difference for whole brain V_T in the cLBP study, with the patients exhibiting higher values than controls ($p < 0.05$; Fig. 1, right). SUV time activity curves from 0 – 90 minutes for each candidate pseudo-reference region are presented in Figure 2.

Target V_T Group Differences

Group comparisons between target V_T yielded a statistically significant difference in thalamus for cLBP patients ($p < 0.05$), and trended towards significance in the precentral gyrus for ALS patients (p=0.051; Fig. 3).

Target SUVR Group Differences

Results from both cohorts indicated that the most significant group differences in target SUVR were obtained using occipital cortex and whole brain as normalizing regions, followed by cerebellum (Fig. 4). ROC curves confirmed that $SUVR_{occip}$ and $SUVR_{WB}$ yielded better sensitivity to detect group differences than $SUVR_{cereb}$ (Fig. 5). $SUVR_{occip}$ displayed the largest area under the ROC curve (AUROC; cLBP: $SUVR_{occip}$ – 0.988, $SUVR_{WB}$ – 0.951, $SUVR_{cereb}$ – 0.840; ALS: $SUVR_{occip}$ – 0.790, $SUVR_{WB}$ – 0.770, $SUVR_{cereb}$ – 0.680). For comparison, Figure 5 also shows the ROC curves obtained using target V_T (AUROC: 0.792 and 0.771 for the cLBP and ALS studies, respectively).

Voxelwise SUVR Group Differences

For both cLBP and ALS cohorts, voxelwise $SUVR_{occip}$ analysis revealed several cortical and subcortical regions exhibiting greater signal in patients than controls (Fig. 6). Several of these regions were consistent with those from the original $SUVR_{WB}$ analyses

[cLBP: thalamus, paracentral lobule, and precentral and postcentral gyri (*14*); ALS: supplementary motor area, corticospinal tract, paracentral lobule, and precentral gyrus (*14*)]. However, using $SUVR_{occip}$, several additional regions with significant group differences emerged [cLBP: posterior insula, striatum, anterior midcingulate and posterior cingulate cortices and others (Supplemental Table 2); ALS: dorsomedial, dorsolateral, ventrolateral, and ventromedial prefrontal cortices, anterior midcingulate cortex and others (Supplemental Table 3)]. Importantly, group differences were present in these same regions for the $SUVR_{WB}$ analysis if the significance threshold was lowered to a significantly less stringent value (Supplemental Fig. 2). There were no regions where SUVR was greater in controls than patients for any pseudo-reference region. There were no significant group differences from the $SUVR_{cereb}$ analysis.

DVR Group Differences

Because the occipital cortex emerged as the preferred pseudo-reference region, based on the results presented above, additional ratio metrics were computed using this brain area only. Group comparisons between target $refDVR_{occip}$ and $blDVR_{occip}$ yielded significant differences between patients and controls for both the CLBP and ALS studies, similar to the V_T and SUVR ROI analyses (Fig. 7).

Associations Across Metrics

Overall, all ratio metrics were highly cross-correlated (Supplemental Table 4), but generally did not correlate well with V_T. Target $SUVR_{occip}$ was strongly correlated with both $refDVR_{occip}$ and $blDVR_{occip}$ for both cLBP and ALS groups (Supplemental Fig. 3), even with plasma outliers included (Supplemental Fig. 4). In the cLBP group, thalamus V_T was significantly correlated with $SUVR_{occip}$ ($p < 0.05$) and $SUVR_{WB}$ ($p < 0.001$), and

showed a trend-level correlation with blDVR$_{occip}$ (p = 0.059). However, there were no other statistically significant correlations between target V_T and SUVR, refDVR$_{occip}$, or blDVR$_{occip}$ (p's ≥ 0.21). Target regions were highly intercorrelated with all reference regions for both V_T and SUV (p's ≤ 1.3 x 10^{-4}). Target and occipital cortex V_T estimated with 2TCM were highly correlated with V_T estimated with Logan graphical analysis (Supplemental Fig. 5).

DISCUSSION

Our study suggests that quantitation of ^{11}C-PBR28 PET signal via pseudo-reference approaches, with or without AIF, can detect group differences with similar sensitivity to analysis with traditional V_T estimates, for the cLBP and ALS datasets presented here. In particular, the occipital cortex emerged as a preferred pseudo-reference region, as it displayed no significant group differences, and relative metrics using occipital cortex as a pseudo-reference region yielded the highest sensitivity to detect group differences in both target ROI and whole-brain voxelwise analyses. Voxelwise differences in ^{11}C-PBR28 SUVR$_{occip}$ were present in the original SUVR$_{WB}$ analyses if the significance threshold was lowered to a much less stringent value (*14,17*). Thus, the use of a localized pseudo-reference region led to increased power to detect group differences. This suggests that spatially diffuse group differences in TSPO signal might contribute to the normalizing signal when using whole brain as a pseudo-reference region. Indeed, we found that whole brain V_T was higher in patients compared to controls, at least for cLBP. This highlights the benefit of using a more focal pseudo-reference region devoid of signal from "target" regions, rather than the use of whole brain or whole gray matter signal, as has been done previously). While additional validation in larger studies is warranted, our observations suggest that occipital cortex may be a suitable

pseudo-reference region for studies involving ^{11}C-PBR28 in these clinical populations, and perhaps in other patient groups in which the occipital cortex is thought to be relatively spared from pathology.

Blood-free methods for quantifying TSPO tracer binding, such as those used in the current study, are extremely attractive for clinical applications. Quantification with kinetic modeling and AIF does not translate well to clinical settings, as it is invasive and requires an experienced practitioner (e.g., an anesthesiologist) to place an arterial catheter. Furthermore, quantifying TSPO tracer binding with V_T (with or without normalization by plasma free fraction (f_P) is associated with large variability that may be attributable to challenges in obtaining accurate blood measurements in addition to physiological variability (*8,18*).

Of note, our criteria for assessing the suitability of analyses using ratio metrics for TSPO imaging included their ability to replicate group differences observed using V_T, as well as their sensitivity to detect group differences in regions where neuroinflammatory is known or expected. Of course, for the latter criterion to be satisfied, the PET signal elevations should match known patterns of glial activation in the disorders under investigation, possibly based on post-mortem or other direct investigations. In ALS, considerable evidence links glial activation to neuropathology (*32*), and post-mortem data have demonstrated a direct association between increased glial activation in the motor cortex and more rapid disease progression (*33*). These in vitro data are supported by numerous in vivo imaging studies (*17,34-36*). As such, ALS presents an excellent opportunity to perform validation studies using the approaches employed in this study. Regarding chronic pain, activation of microglia and/or astrocytes has been reported in the spinal cord in patients with HIV-associated neuropathy (*37*) and complex regional pain syndrome (*38*). While post-mortem data directly demonstrating the spatial pattern of pain-

related immunoactivation in the brain is so far unavailable, several preclinical studies report its occurrence in numerous brain regions, including thalamus, somatosensory cortex, ventral striatum, and ventral tegmental area (*39-41*).

Using occipital cortex normalization, we found that the elevated ^{11}C-PBR28 signal originally reported with $SUVR_{WB}$ (e.g., thalamus, somatosensory and motor cortices in cLBP patients; motor/premotor cortices in ALS patients) became more bilateral and pronounced with $SUVR_{occip}$. Importantly, many of these are regions that have exhibited glial activation in preclinical models of chronic back pain (*39,41*) and in post-mortem and preclinical studies of ALS (*32,33*). Furthermore, in both disease cohorts we observed additional regions of significantly increased PET signal previously observed only well below threshold, and within structures affected by the respective pathologies. In cLBP patients, we observed elevated PET signal in the middle/anterior cingulate cortex (Fig. 5; Supplemental Table 1), in which glial activation has been suggested to underlie the affective component of pain in neuropathic pain models (*42,43*). Additionally, group effects were also detected in the ventral tegmental area and the ventral striatum, reward-processing regions that exhibit microglial activation in animal neuropathic pain models (*40,41*). In ALS patients, voxelwise $SUVR_{occip}$ analysis revealed additional clusters in several regions, including prefrontal regions and anterior cingulate cortex (Fig. 6; Supplemental Table 2), which is in line with recent post-mortem data demonstrating increased inflammatory markers in the frontal cortex of ALS patients (*44*).

We also reported that analysis of both refDVR and blDVR yielded group differences comparable to the analysis with V_T and SUVR, and these outcomes were strongly correlated with SUVR measures. However, correlations between target V_T and relative measures were not as robust as those between relative metrics. Further studies are warranted to investigate the observed dissociation between V_T and ratio metrics.

It is important to stress that due to the large heterogeneity of clinical populations and TSPO tracer kinetics, the results presented here do not necessarily translate to other disorders with a neuroinflammatory component or other TSPO tracers. A cerebellar pseudo-reference region achieved successful group separation in Alzheimer's Disease patients (*4*), but $SUVR_{cereb}$ did not detect similar group differences as with V_T in the current study, or in a recent study of temporal lobe epilepsy (*7*). In the current sample, this is likely due to higher variability in $SUVR_{cereb}$ compared to $SUVR_{occip}$. These discrepant results emphasize the need for separate assessment of each clinical population and tracer of interest.

Several caveats should be considered when interpreting the results of our study. Firstly, we did not measure f_P. However, many previously published studies reported V_T values without correction for f_P (*13,29*), some electing not to incorporate it despite having collected it because of the excessive variability introduced by this measurement (*15,30*). Thus, it is currently unclear whether measurement of f_P is beneficial for ^{11}C-PBR28 quantification. Secondly, studies using relative metrics need to be interpreted cautiously, and require careful validation in large cohorts to ensure the appropriateness of the region selected for pseudo-reference. For a region to be a suitable pseudo-reference, it should not display significant group differences. Although there were no group differences in uptake in our pseudo-reference regions (except for whole brain V_T in the cLBP study), this does not exclude the possibility that small, non-significant differences could bias the outcome measure. There was also a high degree of correlation between target and reference SUV and V_T, which means a large part of the signal is removed from the target region, some of which may be biologically relevant. Finally, recent evidence suggests that vascular TSPO binding may affect quantification (*10*). Given the known heterogeneity of cerebral vascularization (*45*), it is possible that regional differences in vascular physiology

(e.g. density) could affect binding differentially, which could lead to bias with pseudo-reference strategies. However, the contributions of differential vascularization to tracer quantification are not well characterized.

CONCLUSION

In the current study, we present evidence indicating that approaches employing ratio metrics appear to be similarly sensitive to detect pathology-related group differences in ^{11}C-PBR28 signal as classic kinetic modeling techniques, at least for the populations evaluated here. However, the reasons behind the largely non-significant associations between relative metrics and V_T needs to be further elucidated. The occipital cortex emerged as the preferred pseudo-reference region, as its signal was not significantly different across groups, and all ratio metrics based on the signal from this region detected group differences similar to those detected by V_T, In addition, in the voxelwise analysis, $SUVR_{occip}$ identified regions of increased glial activation that included those detected from the initial analyses, as well as several additional regions that were relevant to the respective pathologies and have been shown to exhibit glial activation in preclinical models and/or post-mortem data. It is important to stress that caveats should be kept in mind when using relative measures, and that the choice of an appropriate pseudo-reference region needs to be pathology-dependent and may not be possible in some cases (e.g., where neuroinflammation is expected to span the entire brain parenchyma). In general, these techniques will require additional validation before widespread use.

ACKNOWLEDGMENTS

We would like to acknowledge Drs. Ciprian Catana and Dan Chonde for help with image processing, and Drs. Vitaly Napadow and Rob Edwards for helpful discussion.

DISCLOSURE

No authors report any conflicts of interest. Funding sources: 1R01NS094306-01A1 (MLL), 1R21NS087472-01A1 (MLL), IASP Early Career Award (MLL), DoD W81XWH-14-1-0543 (MLL), Harvard Catalyst Advanced Imaging Pilot Grant (JMH), a sponsored research agreement with Eli Lilly (JMH), K23NS083715 (NA), 5T32EB13180 (T32 supporting DSA), and an Anne Young Fellowship (NA).

REFERENCES

1. Albrecht DS, Granziera C, Hooker JM, Loggia ML. In vivo imaging of human neuroinflammation. *ACS Chem Neurosci.* 2016;7:470-483.

2. Liu GJ, Middleton RJ, Hatty CR, et al. The 18 kDa translocator protein, microglia and neuroinflammation. *Brain Pathol.* 2014;24:631-653.

3. Chen MK, Guilarte TR. Translocator protein 18 kDa (TSPO): molecular sensor of brain injury and repair. *Pharmacol Ther.* 2008;118:1-17.

4. Lyoo CH, Ikawa M, Liow JS, et al. Cerebellum can serve as a pseudo-reference region in alzheimer disease to detect neuroinflammation measured with PET radioligand binding to translocator protein. *J Nucl Med.* 2015;56:701-706.

5. Kreisl WC, Lyoo CH, McGwier M, et al. In vivo radioligand binding to translocator protein correlates with severity of Alzheimer's disease. *Brain.* 2013;136:2228-2238.

6. Vera JH, Guo Q, Cole JH, et al. Neuroinflammation in treated HIV-positive individuals: A TSPO PET study. *Neurology.* 2016;86:1425-1432.

7. Gershen LD, Zanotti-Fregonara P, Dustin IH, et al. Neuroinflammation in temporal lobe epilepsy measured using positron emission tomographic imaging of translocator protein. *JAMA Neurol.* 2015;72:882-888.

8. Owen DR, Guo Q, Rabiner EA, Gunn RN. The impact of the rs6971 polymorphism in TSPO for quantification and study design. *Clin Transl Imaging.* 2015;3:1-6.

9. Kreisl WC, Jenko KJ, Hines CS, et al. A genetic polymorphism for translocator protein 18 kDa affects both in vitro and in vivo radioligand binding in human brain to this putative biomarker of neuroinflammation. *J Cereb Blood Flow Metab.* 2013;33:53-58.

10. Rizzo G, Veronese M, Tonietto M, Zanotti-Fregonara P, Turkheimer FE, Bertoldo A. Kinetic modeling without accounting for the vascular component impairs the quantification of [(11)C]PBR28 brain PET data. *J Cereb Blood Flow Metab.* 2014;34:1060-1069.

11. Lockhart A, Davis B, Matthews JC, et al. The peripheral benzodiazepine receptor ligand PK11195 binds with high affinity to the acute phase reactant alpha1-acid glycoprotein: implications for the use of the ligand as a CNS inflammatory marker. *Nucl Med Biol.* 2003;30:199-206.

12. Owen DR, Yeo AJ, Gunn RN, et al. An 18-kDa translocator protein (TSPO) polymorphism explains differences in binding affinity of the PET radioligand PBR28. *J Cereb Blood Flow Metab.* 2012;32:1-5.

13. Yoder KK, Territo PR, Hutchins GD, et al. Comparison of standardized uptake values with volume of distribution for quantitation of [(11)C]PBR28 brain uptake. *Nucl Med Biol.* 2015;42:305-308.

14. Loggia ML, Chonde DB, Akeju O, et al. Evidence for brain glial activation in chronic pain patients. *Brain.* 2015;138(pt. 3):604-615.

15. Bloomfield PS, Selvaraj S, Veronese M, et al. Microglial activity in people at ultra high risk of psychosis and in schizophrenia: an [(11)C]PBR28 PET brain imaging study. *Am J Psychiatry.* 2016;173:44-52.

16. Coughlin JM, Wang Y, Munro CA, et al. Neuroinflammation and brain atrophy in former NFL players: An in vivo multimodal imaging pilot study. *Neurobiol Dis.* 2015;74:58-65.

17. Zurcher NR, Loggia ML, Lawson R, et al. Increased in vivo glial activation in patients with amyotrophic lateral sclerosis: assessed with [(11)C]-PBR28. *Neuroimage Clin.* 2015;7:409-414.

18. Turkheimer Federico E, Rizzo G, Bloomfield Peter S, et al. The methodology of TSPO imaging with positron emission tomography. *Biochem Soc Trans.* 2015;43:586-592.

19. Fujita M, Imaizumi M, Zoghbi SS, et al. Kinetic analysis in healthy humans of a novel positron emission tomography radioligand to image the peripheral benzodiazepine receptor, a potential biomarker for inflammation. *Neuroimage.* 2008;40:43-52.

20. Cauda F, Palermo S, Costa T, et al. Gray matter alterations in chronic pain: A network-oriented meta-analytic approach. *Neuroimage Clin.* 2014;4:676-686.

21. Kregel J, Meeus M, Malfliet A, et al. Structural and functional brain abnormalities in chronic low back pain: A systematic review. *Semin Arthritis Rheum.* 2015;45:229-237.

22. Foerster BR, Welsh RC, Feldman EL. 25 years of neuroimaging in amyotrophic lateral sclerosis. *Nat Rev Neurol.* 2013;9:513-524.

23. Petri S, Kollewe K, Grothe C, et al. GABA(A)-receptor mRNA expression in the prefrontal and temporal cortex of ALS patients. *J Neurol Sci.* 2006;250:124-132.

24. Kolb A, Wehrl HF, Hofmann M, et al. Technical performance evaluation of a human brain PET/MRI system. *Eur Radiol.* 2012;22:1776-1788.

25. Izquierdo-Garcia D, Hansen AE, Forster S, et al. An SPM8-based approach for attenuation correction combining segmentation and nonrigid template formation: application to simultaneous PET/MR brain imaging. *J Nucl Med.* 2014;55:1825-1830.

26. Leys C, Ley C, Klein O, Bernard P, Licata L. Detecting outliers: Do not use standard deviation around the mean, use absolute deviation around the median. *J Exp Soc Psychol.* 2013;4:764-766.

27. Logan J, Fowler JS, Volkow ND, Wang GJ, Ding YS, Alexoff DL. Distribution volume ratios without blood sampling from graphical analysis of PET data. *J Cereb Blood Flow Metab.* 1996;16:834-840.

28. Logan J, Fowler JS, Volkow ND, et al. Graphical analysis of reversible radioligand binding from time-activity measurements applied to [N-11C-methyl]-(-)-cocaine PET studies in human subjects. *J Cereb Blood Flow Metab.* 1990;10:740-747.

29. Fujita M, Mahanty S, Zoghbi SS, et al. PET reveals inflammation around calcified Taenia solium granulomas with perilesional edema. *PLoS One.* 2013;8:e74052.

30. Hines CS, Fujita M, Zoghbi SS, et al. Propofol decreases in vivo binding of 11C-PBR28 to translocator protein (18 kDa) in the human brain. *J Nucl Med.* 2013;54:64-69.

31. Smith SM, Nichols TE. Threshold-free cluster enhancement: addressing problems of smoothing, threshold dependence and localisation in cluster inference. *Neuroimage.* 2009;44:83-98.

32. Philips T, Robberecht W. Neuroinflammation in amyotrophic lateral sclerosis: role of glial activation in motor neuron disease. *Lancet Neurol.* 2011;10:253-263.

33. Brettschneider J, Toledo JB, Van Deerlin VM, et al. Microglial activation correlates with disease progression and upper motor neuron clinical symptoms in amyotrophic lateral sclerosis. *PLoS One.* 2012;7:e39216.

34. Turner MR, Cagnin A, Turkheimer FE, et al. Evidence of widespread cerebral microglial activation in amyotrophic lateral sclerosis: an [11C](R)-PK11195 positron emission tomography study. *Neurobiol Dis.* 2004;15:601-609.

35. Corcia P, Tauber C, Vercoullie J, et al. Molecular imaging of microglial activation in amyotrophic lateral sclerosis. *PLoS One.* 2012;7:e52941.

36. Alshikho MJ, Zurcher NR, Loggia ML, et al. Glial activation colocalizes with structural abnormalities in amyotrophic lateral sclerosis. *Neurology.* 2016;87:2554-2561.

37. Shi Y, Gelman BB, Lisinicchia JG, Tang SJ. Chronic-pain-associated astrocytic reaction in the spinal cord dorsal horn of human immunodeficiency virus-infected patients. *J Neurosci.* 2012;32:10833-10840.

38. Del Valle L, Schwartzman RJ, Alexander G. Spinal cord histopathological alterations in a patient with longstanding complex regional pain syndrome. *Brain Behav Immun.* 2009;23:85-91.

39. LeBlanc BW, Zerah ML, Kadasi LM, Chai N, Saab CY. Minocycline injection in the ventral posterolateral thalamus reverses microglial reactivity and thermal hyperalgesia secondary to sciatic neuropathy. *Neurosci Lett.* 2011;498:138-142.

40. Taylor AM, Castonguay A, Taylor AJ, et al. Microglia disrupt mesolimbic reward circuitry in chronic pain. *J Neurosci.* 2015;35:8442-8450.

41. Taylor AM, Mehrabani S, Liu S, Taylor AJ, Cahill CM. Topography of microglial activation in sensory- and affect-related brain regions in chronic pain. *J Neurosci Res.* August 3, 2016 [Epub ahead of print].

42. Chen FL, Dong YL, Zhang ZJ, et al. Activation of astrocytes in the anterior cingulate cortex contributes to the affective component of pain in an inflammatory pain model. *Brain Res Bull.* 2012;87:60-66.

43. Di Cesare Mannelli L, Pacini A, Bonaccini L, Zanardelli M, Mello T, Ghelardini C. Morphologic features and glial activation in rat oxaliplatin-dependent neuropathic pain. *J Pain.* 2013;14:1585-1600.

44. Berjaoui S, Povedano M, Garcia-Esparcia P, Carmona M, Aso E, Ferrer I. Complex inflammation mRNA-related response in ALS Is region dependent. *Neural Plast.* 2015;2015:573784.

45. Duvernoy HM, Delon S, Vannson JL. Cortical blood vessels of the human brain. *Brain Res Bull.* 1981;7:519-579.

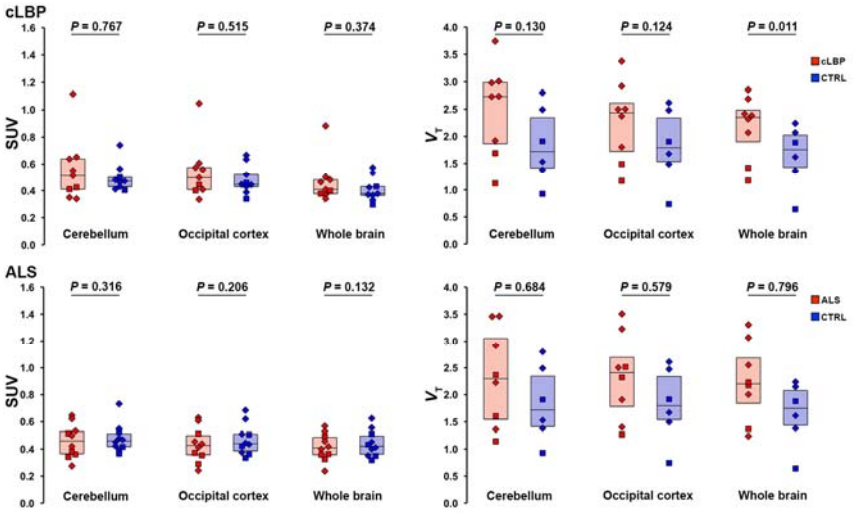

FIGURE 1. Group comparison of SUV (left) and V_T (right) from candidate pseudo-reference regions evaluated in this work. Boxes represent the 25%- 75% interquartile range; horizontal line represents the median. Diamonds represent subjects with the high-affinity *TSPO* genotype (Ala/Ala in the Ala147Thr *TSPO* polymorphism), squares represent subjects with mixed-affinity genotype (Ala/Thr).

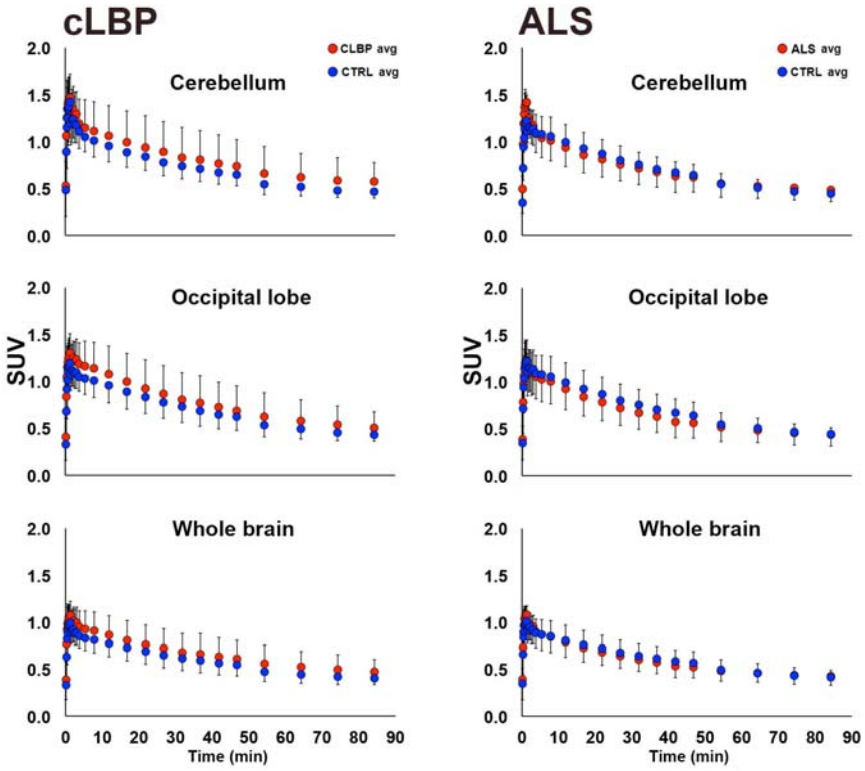

FIGURE 2. Group comparison of 0-90 minute time activity curves for candidate pseudo-reference regions. Each data point represents the average within-group SUV for that time point ± SD. In the cLBP plots (left) both patients matching the same control subject are included.

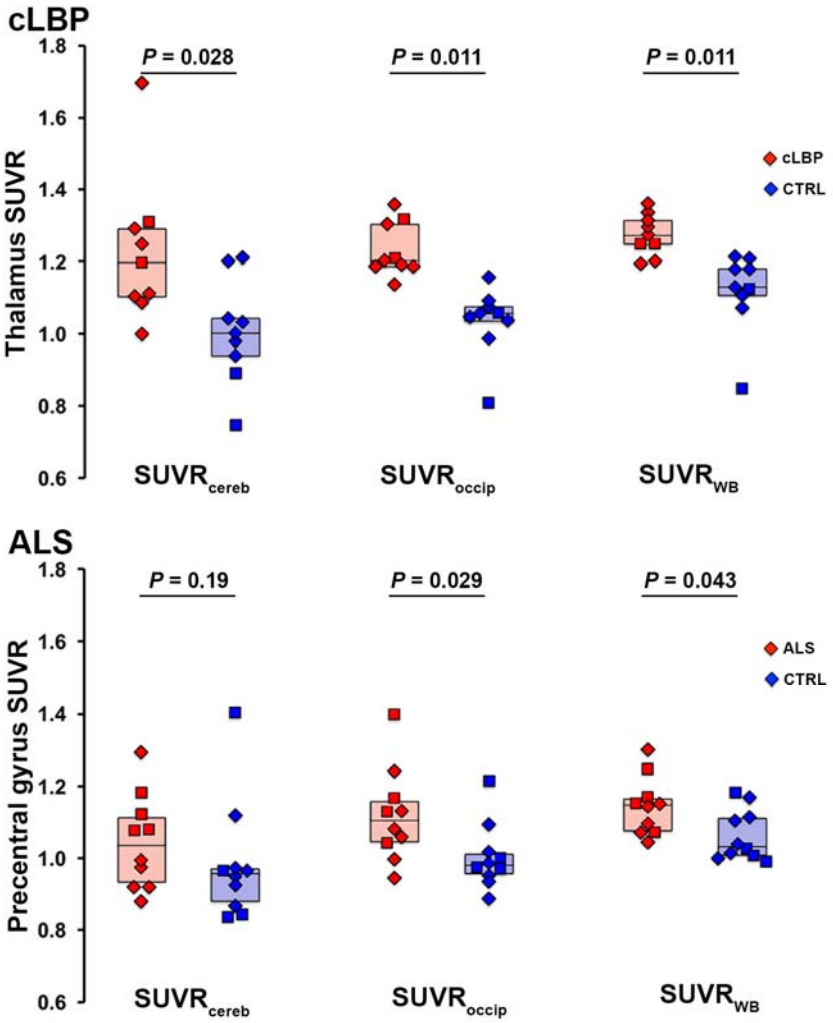

FIGURE 3. Group comparison of target V_T estimates for cLBP (top) and ALS (bottom) groups.

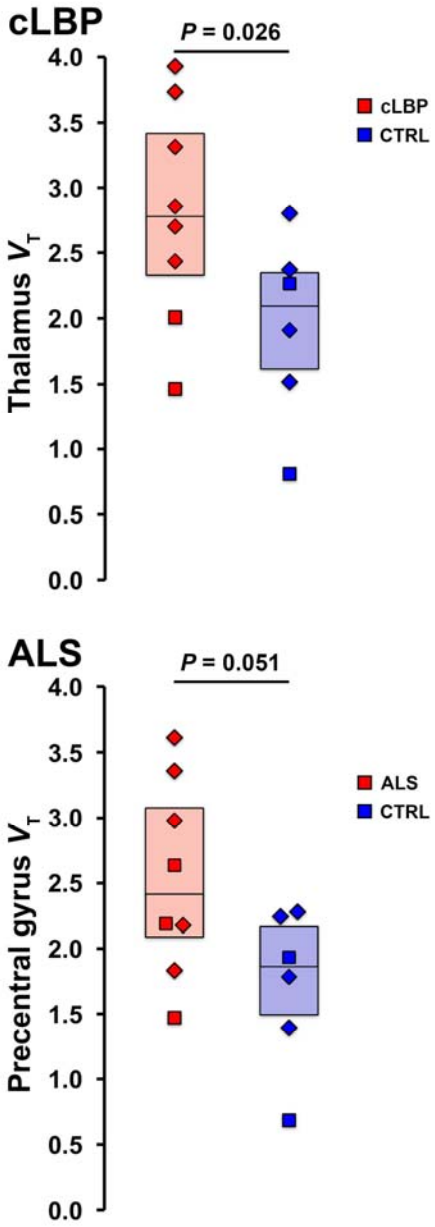

FIGURE 4. Group differences in target SUVR for each pseudo-reference region. Horizontal bars represent group median. In the cLBP plots (top) both patients matching the same control subject are included as data points, but the median value reflects only the best matching patient included.

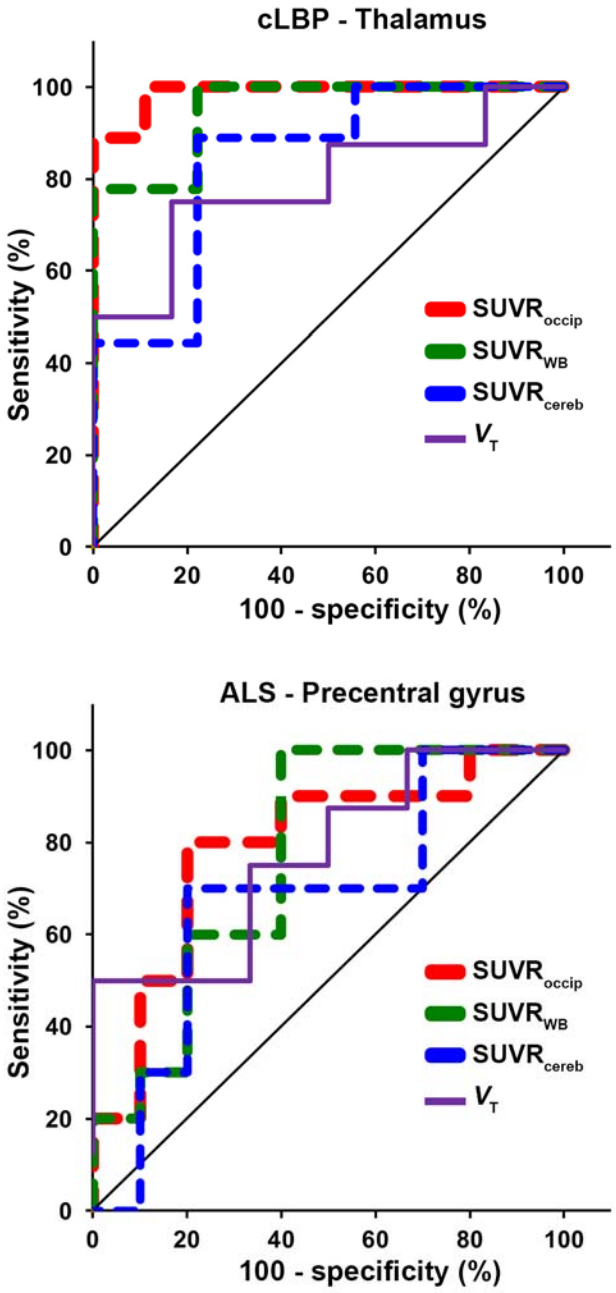

FIGURE 5. Receiver operating characteristic (ROC) curves of target SUVR (dashed lines) and V_T (solid line) for each pseudo-reference region. Line of identity (chance, no discriminatory power) is shown in black.

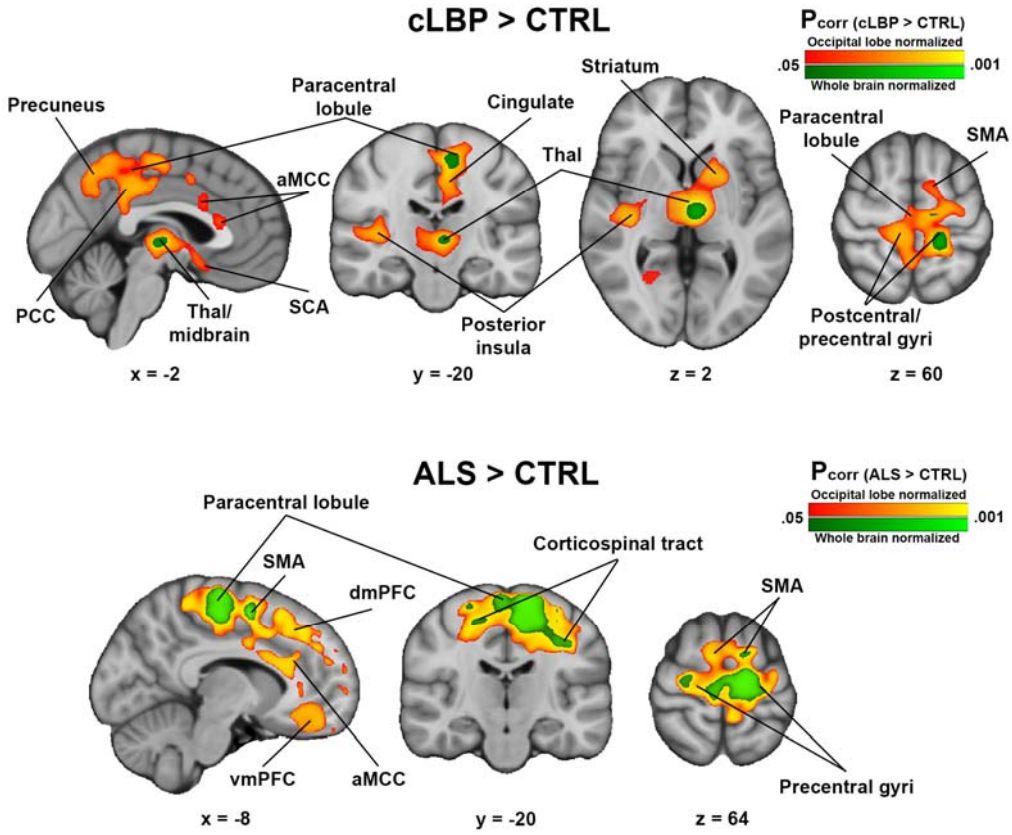

FIGURE 6. Regions of elevated ^{11}C-PBR28 SUVR in patients compared to controls. Results from $SUVR_{WB}$ analyses (analyses from the original studies) are shown in green colorscale, $SUVR_{occip}$ results are shown in red-yellow colorscale. Top: cLBP > controls Bottom: ALS > controls. No regions was significant in either cLBP < controls or ALS < controls contrasts. PCC – posterior cingulate cortex; aMCC – anterior midcingulate cortex; SCA – subcallosal area; Thal – thalamus; SMA – supplementary motor area; dmPFC – dorsomedial prefrontal cortex; vmPFC – ventromedial prefrontal cortex.

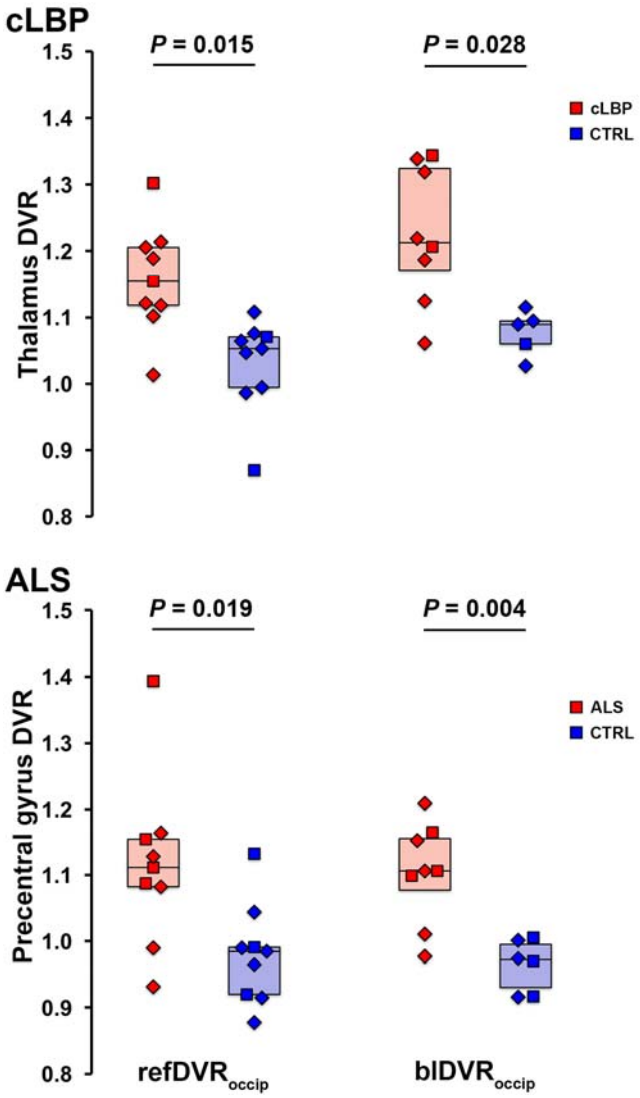

FIGURE 7. Group comparison of $refDVR_{occip}$ and $blDVR_{occip}$. Horizontal bars represent group median.

Measure	cLBP	CON (cLBP)	ALS	CON (ALS)
SUV				
Target	0.698 ± 0.25 (35.8%)	0.525 ± 0.15 (28.6%)	0.495 ± 0.11 (22.2%)	0.488 ± 0.12 (24.6%)
Whole brain	0.470 ± 0.16 (34.0%)	0.412 ± 0.09 (21.8%)	0.416 ± 0.10 (24.0%)	0.441 ± 0.10 (22.7%)
Occipital	0.542 ± 0.21 (38.7%)	0.482 ± 0.11 (22.8%)	0.432 ± 0.13 (30.1%)	0.470 ± 0.11 (23.4%)
Cerebellum	0.556 ± 0.24 (43.2%)	0.497 ± 0.10 (20.1%)	0.460 ± 0.12 (26.1%)	0.480 ± 0.10 (20.8%)
V_T				
Target	2.81 ± 0.84 (29.9%)	1.95 ± 0.71 (36.4%)	2.53 ± 0.75 (29.6%)	1.72 ± 0.60 (34.9%)
Whole brain	2.17 ± 0.59 (27.2%)	1.64 ± 0.58 (35.4%)	2.24 ± 0.73 (32.6%)	1.65 ± 0.59 (35.8%)
Occipital	2.27 ± 0.74 (32.6%)	1.82 ± 0.69 (37.9%)	2.33 ± 0.80 (34.3%)	1.82 ± 0.68 (37.4%)
Cerebellum	2.49 ± 0.85 (34.1%)	1.84 ± 0.71 (38.6%)	2.32 ± 0.91 (39.2%)	1.84 ± 0.71 (38.6%)
SUVR				
$SUVR_{WB}$	1.27 ± 0.06 (4.72%)	1.12 ± 0.11 (9.82%)	1.14 ± 0.08 (7.02%)	1.06 ± 0.07 (6.60%)
$SUVR_{occip}$	1.23 ± 0.07 (5.69%)	1.03 ± 0.10 (9.71%)	1.12 ± 0.13 (11.6%)	1.00 ± 0.09 (9.00%)
$SUVR_{cereb}$	1.22 ± 0.20 (16.4%)	1.00 ± 0.14 (14.0%)	1.04 ± 0.13 (12.5%)	0.984 ± 0.17 (17.3%)
$refDVR_{occip}$	1.16 ± 0.08 (6.70%)	1.03 ± 0.16 (15.5%)	1.11 ± 0.12 (10.8%)	0.980 ± 0.08 (8.16%)
$blDVR_{occip}$	1.25 ± 0.11 (8.80%)	1.08 ± 0.10 (9.26%)	1.11 ± 0.13 (11.7%)	0.951 ± 0.07 (7.36%)

TABLE 1. Descriptive statistics for all outcome measures. Values are mean ± S.D., with %COV shown in parentheses below. “Target” refers to regions showing the largest group differences in the original studies; bilateral thalamus (cLBP) and bilateral precentral gyrus (ALS). Values for blood-based measures (V_T and blDVR) exclude plasma outlier subjects.

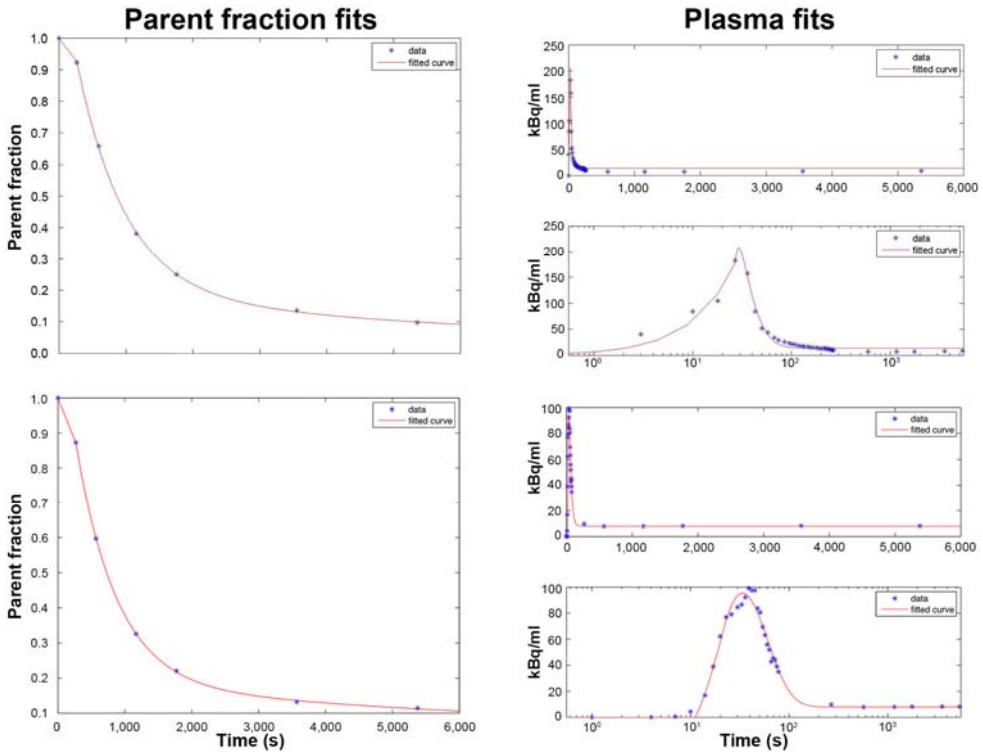

SUPPLEMENTAL FIGURE 1. Examples of model fitting for parent fraction and plasma activity for two representative subjects. Actual datapoints are shown as blue stars, exponential model fit of the data is shown as a red line. Left: parent fraction fits for a control subject (top) and patient (bottom). Right: plasma activity fits for a control subject (top) and patient (bottom). The bottom subpanel is on a logarithmic scale to show fitting of the peak.

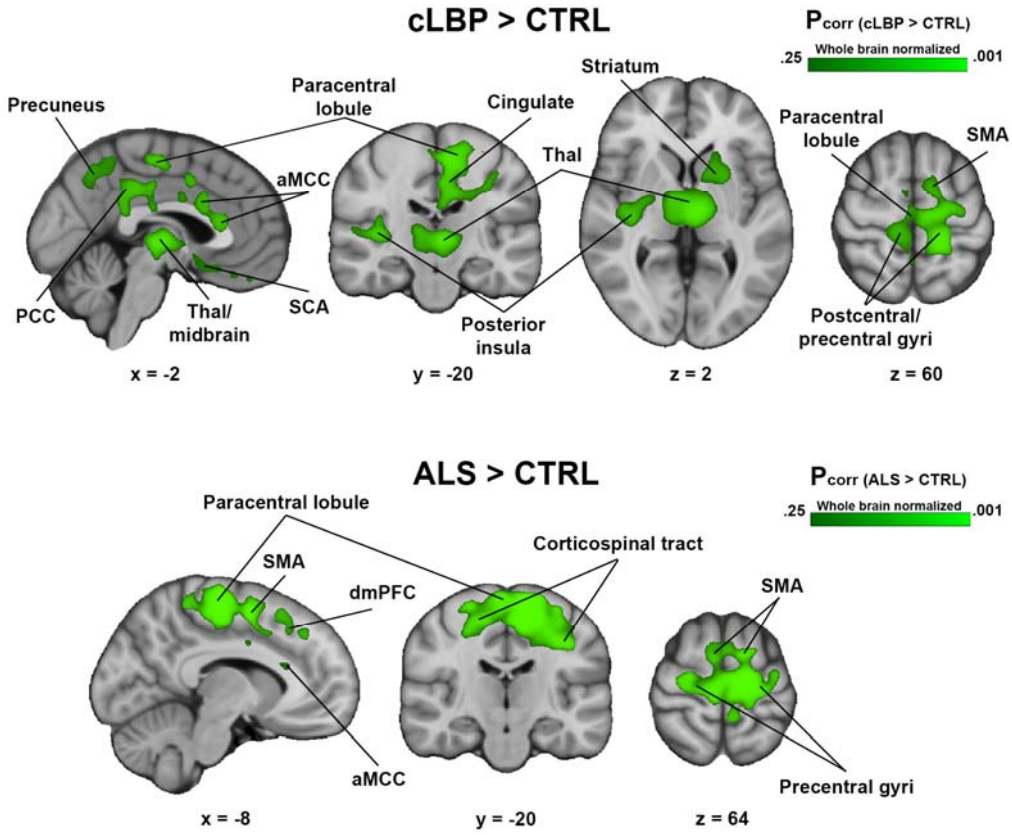

SUPPLEMENTAL FIGURE 2. Regions of elevated ^{11}C-PBR28 $SUVR_{WB}$ in patients compared to controls, visualized at an extremely lenient statistical threshold ($p<0.25$). These results show group differences highly overlapping with those observed at strict threshold with the $SUVR_{occip}$ analyses (Fig. 5). Top: cLBP > controls. Bottom: ALS > controls. No region was significant in either the cLBP < controls or ALS < controls contrasts.

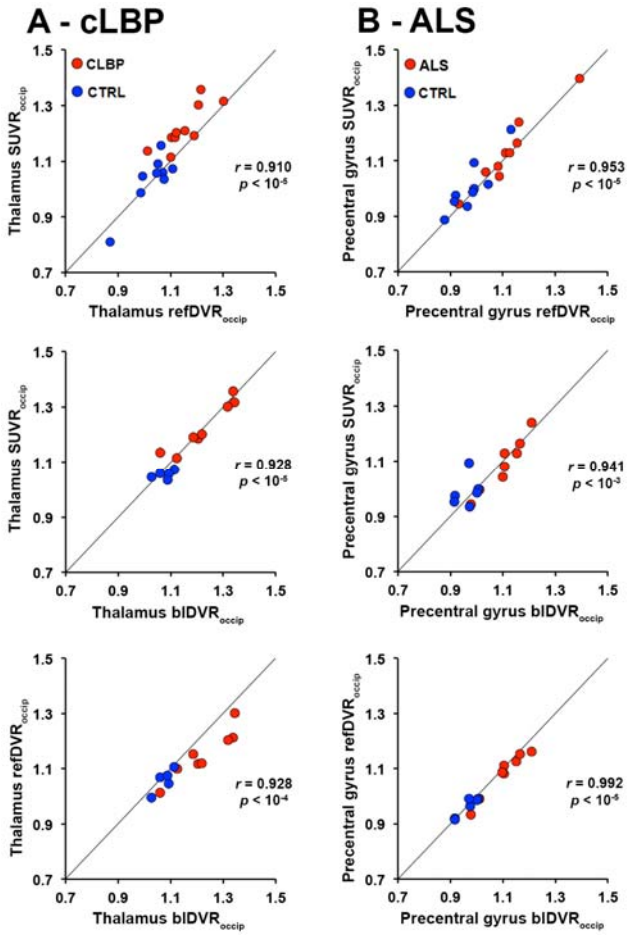

SUPPLEMENTAL FIGURE 3. Relationship between target $SUVR_{occip}$, $refDVR_{occip}$, and $bIDVR_{occip}$. Line of identity is shown in black.

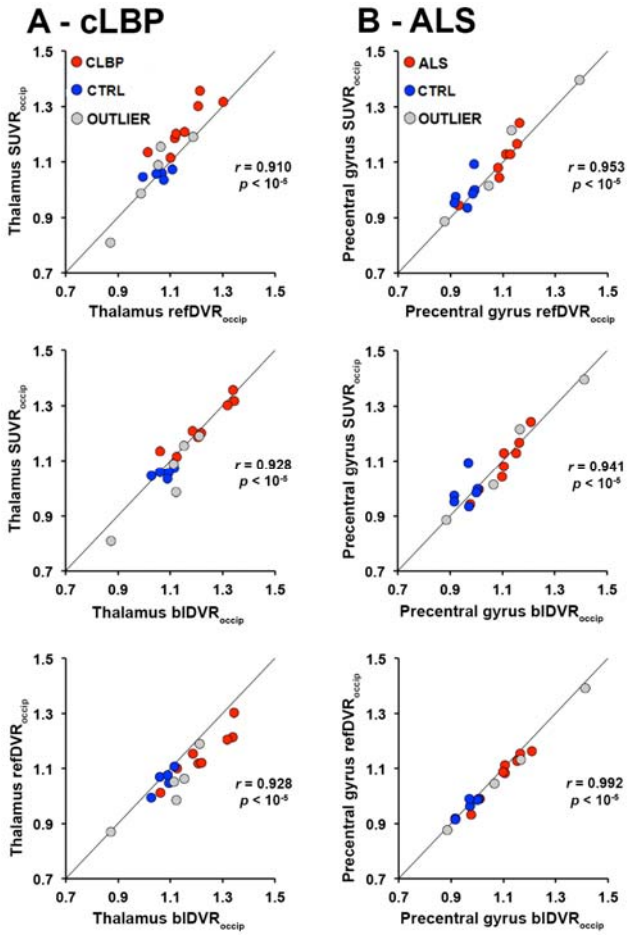

SUPPLEMENTAL FIGURE 4. Relationship between target $SUVR_{occip}$, $refDVR_{occip}$, and $blDVR_{occip}$, plasma outliers included and identified. Line of identity is shown in black.

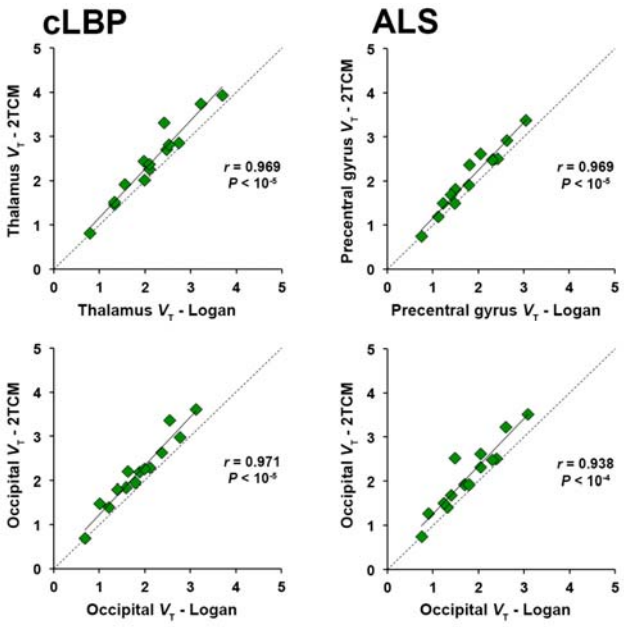

SUPPLEMENTAL FIGURE 5. Relationship between Logan and 2TCM estimations of target and occipital cortex V_T. Line of identity is shown as a dotted diagonal line. Plasma outliers are not included.

SUPPLEMENTAL TABLE 1. Subject demographics

	cLBP	CON (cLBP)	ALS	CON (ALS)
N	10	9	10	10
Sex	5M/5F	5M/4F	6M/4F	6M/4F
TSPO Genotype	7 Ala/Ala; 3 Ala/Thr	7 Ala/Ala; 2 Ala/Thr	6 Ala/Ala; 4 Ala/Thr	6 Ala/Ala; 4 Ala/Thr
Age (years)	48.9 (12)	49.6 (12)	53.2 (11)	51.1 (11)
Injected Dose (MBq)	409.5 (27.9)	407.4 (15.4)	429.7 (33.8)	424.5 (42)
Injected mass (nmol/kg)	0.06 (0.02)	0.10 (0.07)	0.06 (0.02)	0.11 (0.07)

Values shown are mean ± standard deviation.

SUPPLEMENTAL TABLE 2. Regions of voxelwise increases in [^{11}C]PBR28 $SUVR_{occip}$ in cLBP patients compared to controls.

		MNI coordinates (mm)			
Region	*P*-value (corr)	X	Y	Z	Cluster size (# voxels)
L Thalamus	0.006	-4	-18	0	1871
R Thalamus	0.016	2	-18	0	
L Putamen	0.021	-22	6	2	
L Caudate	0.029	-14	14	6	
L Subcallosal area	0.033	-4	14	-16	
L Ventral striatum	0.035	-6	8	-6	
L Paracentral lobule	0.008	-8	-22	50	7236
L Postcentral gyrus	0.008	-18	-38	64	
L Posterior midcingulate cortex	0.012	-6	-20	44	
L Precentral gyrus	0.016	-26	-12	56	
R Paracentral lobule	0.016	6	-32	58	
L/R Posterior cingulate cortex	0.018	0	-40	30	
R Precuneus	0.018	6	-58	50	
L Precuneus	0.020	-4	-60	38	
R Postcentral gyrus	0.020	24	-30	66	
R Precentral gyrus	0.021	20	-28	64	

R Supramarginal gyrus	0.021	36	-50	38	
L Internal capsule	0.021	-16	12	2	
L Pre-supplementary motor area	0.027	-8	2	48	
R Angular gyrus	0.029	30	-70	28	
Ventral tegmental area	0.033	0	-18	-8	
R Pre-supplementary motor area	0.035	6	12	48	
L Anterior midcingulate cortex	0.035	-4	14	28	
Corpus callosum	0.035	-4	22	14	
L Supramarginal gyrus	0.049	-36	-42	40	
R Posterior Insula	0.018	36	-20	6	747
S2	0.027	36	-28	18	

SUPPLEMENTAL TABLE 3. Regions of voxelwise increases in [^{11}C]PBR28 $SUVR_{occip}$ in ALS patients compared to controls.

		MNI coordinates (mm)			
Region	*P*-value (corr)	X	Y	Z	Cluster size (# voxels)
L Precentral gyrus	0.000	-12	-20	62	21809
L Superior frontal gyrus	0.002	-16	-6	58	
L Paracentral lobule	0.003	-2	-12	52	
L Postcentral gyrus	0.003	-26	-30	52	
L Supplementary motor area	0.003	-4	2	54	
R Precentral gyrus	0.004	24	-14	60	
R Paracentral lobule	0.004	4	-20	64	
R Supplementary motor area	0.004	10	2	60	
R Superior frontal gyrus	0.004	22	8	46	
L Corticospinal tract	0.004	-24	-24	42	
L Middle frontal gyrus	0.007	-26	14	46	
L Ventrolateral prefrontal cortex	0.007	-24	56	-2	
L Orbital gyrus	0.008	-30	26	-20	
L Dorsolateral prefrontal cortex	0.008	-34	40	26	
L Anterior midcingulate cortex/corpus callosum	0.008	-6	24	18	
L Frontoinsular cortex	0.010	-34	24	0	

R Anterior midcingulate cortex	0.013	6	14	32	
L Ventromedial prefrontal cortex	0.014	-4	42	-12	
Dorsomedial prefrontal cortex	0.016	0	60	18	
R Pregenual anterior cingulate cortex	0.019	12	44	-2	
R Orbital gyrus	0.047	14	26	-22	28

SUPPLEMENTAL TABLE 4. Interregional correlations between target and reference SUV and V_T.

Correlation between target and reference region SUV and V_T					
Target and reference SUV					
Target region	Reference region	**Control**		**Patient**	
		r-value	*p*-value	*r*-value	*p*-value
Thalamus (CLBP dataset)	Occipital cortex	0.956	1.6×10^{-5}	0.988	$< 1 \times 10^{-6}$
	Whole brain	0.922	1.4×10^{-4}	0.961	1×10^{-5}
	Cerebellum	0.881	7.5×10^{-4}	0.948	3×10^{-5}
Precentral gyrus (ALS dataset)	Occipital cortex	0.941	4.8×10^{-4}	0.931	9.3×10^{-5}
	Whole brain	0.962	9.0×10^{-6}	0.950	2.6×10^{-5}
	Cerebellum	0.829	3.0×10^{-3}	0.873	9.7×10^{-4}
Target and reference V_T					
Target region	Reference region	**Control**		**Patient**	
		r-value	*p*-value	*r*-value	*p*-value
Thalamus (CLBP dataset)	Occipital cortex	0.947	4.1×10^{-3}	0.956	2.0×10^{-4}
	Whole brain	0.992	1.1×10^{-4}	0.962	1.4×10^{-4}
	Cerebellum	0.949	3.8×10^{-3}	0.904	2.0×10^{-3}
Precentral gyrus (ALS dataset)	Occipital cortex	0.974	1.0×10^{-3}	0.949	3.2×10^{-4}
	Whole brain	0.996	2.6×10^{-5}	0.952	2.7×10^{-4}
	Cerebellum	0.925	8.2×10^{-3}	0.975	3.6×10^{-5}

The Journal of NUCLEAR MEDICINE

Pseudo-reference regions for glial imaging with ^{11}C-PBR28: investigation in two clinical cohorts

Daniel Strakis Albrecht, Marc David Normandin, Sergey Shcherbinin, Dustin W. Wooten, Adam J. Schwarz, Nicole R. Zurcher, Vanessa N. Barth, Nicolas J. Guehl, Oluwaseun Johnson-Akeju, Nazem Atassi, Mattia Veronese, Federico Turkheimer, Jacob M. Hooker and Marco Luciano Loggia

J Nucl Med.
Published online: August 17, 2017.
Doi: 10.2967/jnumed.116.178335

The Journal of Nuclear Medicine is published monthly.
SNMMI | Society of Nuclear Medicine and Molecular Imaging
1850 Samuel Morse Drive, Reston, VA 20190.
(Print ISSN: 0161-5505, Online ISSN: 2159-662X)

SNMMI SOCIETY OF NUCLEAR MEDICINE AND MOLECULAR IMAGING